7-2018

Thermodynamic and Kinetic study of the removal of Cu2+ and Pb2+ ions from aqueous solution using Fe7S8 nanomaterial

Jesus Cantu
The University of Texas Rio Grande Valley

Diego F. Gonzalez
The University of Texas Rio Grande Valley

Yvette Cantu
The University of Texas Rio Grande Valley

Thomas Eubanks
The University of Texas Rio Grande Valley

Jason Parsons
The University of Texas Rio Grande Valley, jason.parsons@utrgv.edu

Recommended Citation

Cantu, J., Gonzalez, D. F., Cantu, Y., Eubanks, T., & Parsons, J. G. (2018). Thermodynamic and Kinetic study of the removal of Cu2+ and Pb2+ ions from aqueous solution using Fe7S8 nanomaterial. Microchemical journal : devoted to the application of microtechniques in all branches of science, 140, 80–86. https://doi.org/10.1016/j.microc.2018.04.003

HHS Public Access

Author manuscript

Microchem J. Author manuscript; available in PMC 2019 July 01.

Published in final edited form as:

Microchem J. 2018 July ; 140: 80–86. doi:10.1016/j.microc.2018.04.003.

Thermodynamic and Kinetic study of the removal of Cu^{2+} and Pb^{2+} ions from aqueous solution using Fe_7S_8 nanomaterial

Jesus Cantu[1], **Diego F. Gonzalez**[1], **Yvette Cantu**[1], **Tom Eubanks**[1], and **J.G. Parsons**[*,1,2]

[1]Department of Chemistry University of Texas Rio Grande Valley 1 West University Blvd. Brownsville TX78521

[2]School of Earth Environmental and Marine Science University of Texas Rio Grande Valley 1 West University Blvd. Brownsville TX78521

Abstract

In the present study, pyrrhotite (Fe_7S_8) was investigated for the removal of Pb^{2+} and $Cu2^{+}$ ions from aqueous solution. The Fe_7S_8 material was prepared through a solvothermal method and was characterized using XRD. The average particle size for the nanomaterial was determined to be 29.86 ± 0.87 nm using XRD analysis and Scherrer's equation. Batch studies were performed to investigate the effects of pH, time, temperature, interfering ions, and the binding capacity of Pb^{2+} and Cu^{2+} ions to the Fe_7S_8 nanomaterial. During the pH profile studies, the optimum pH for the binding of Pb^{2+} and Cu^{2+} was determined to be pH 5 for both cations. Isotherm studies were conducted from which the thermodynamics and binding capacities for both Cu^{2+} and Pb^{2+} were determined. The binding capacity for Pb^{2+} and Cu^{2+} binding to the Fe_7S_8 were determined to be 0.039 and 0.102 mmol/g, respectively at 25°C. The thermodynamic parameters indicated a ΔG for the sorption of Pb^{2+} ranged from 5.07 kJ/mol to −2.45 kJ/mol indicating a non-spontaneous process was occurring. Whereas, the ΔG for Cu^{2+} ion binding ranged from 9.78 kJ/mol to −11.23 kJ/mol indicating a spontaneous process at higher temperatures. The enthalpy indicated an endothermic reaction was occurring for the binding of Pb^{2+} and Cu^{2+} to the Fe_7S_8 nanomaterial with ΔH values of 55.8 kJ/mol and 153.5 kJ/mol, respectively. Furthermore, the ΔS values for the reactions were positive indicating an increase in the entropy of the system after metal ion binding. Activation energy studies indicated the binding for both Pb^{2+} and Cu^{2+} occurred through chemisorption.

1. Introduction

The Earth is made up of approximately 71% water in which 97% of that is saltwater and 2.5–2.75% is fresh water. The fresh water on the planet is distributed between glaciers (68.7%), ground water (30.1%), and surface water (1.2%) [1]. However, rapid industrialization, potable water contamination has become a global concern with respect to

*Corresponding author. Tel.:+1 956 882 7772, jason.parsons@utrgv.edu.

human health and environmental health. Anthropogenic contamination of water systems fall under one of two broad chemical classifications, which are inorganic and organic. The contaminates include compounds such as pesticides, herbicides, petroleum byproducts, detergents, and inorganic pollutants such as: heavy metal ions, fertilizers, and acid wastes. Many of the metals released from anthropogenic processes in to the environment are heavy metals, which are generally toxic. Lead and copper are two elements of interest due to the health issues related to the exposure of these elements.

Lead does not have a biological role in the human body. Pb is commonly found as a divalent cation that can strongly binds to proteins though different functional groups. Exposure to lead has been shown to affect the nervous system, production of hemoglobin, and renal system. At low concentrations, Pb has been found to compete with calcium binding with phosphokinase C affecting neuronal signaling; Pb further inhibits calcium from entering cells. [2] It is of most concern for children who upon exposure can absorb 4–5 times more lead than adults [3,4]. In adults, lead targets the kidneys, blood pressure, and the peripheral and central nervous systems (PNS and CNS) [2,5]. However, on the other hand, copper is an essential trace element and is needed at low concentrations for proper biological function. For instance, it is used in enzymes such as: tyrosinase, p-hydroxyphenyl pyruvate hydrolase, and cytochrome c oxidase, which are used for growth and development [6]. At high concentrations, it is toxic to the body and it primarily leads to liver toxicity. It can further cause lesions to the central nervous system, abdominal pain, and diarrhea [7-10]. In early stages, high amounts of copper can cause lethargy, weakness, and anorexia [6].

Current techniques for the removal of heavy metals from aqueous systems include but are not limited to: precipitation, ion exchange, liquid-liquid extraction, biosorption, and adsorption [11,12]. Even though, these techniques have shown to be effective in removal of heavy metals from aqueous solution, the implementation of many these technologies tend to be either costly or complicated. For instance, precipitating agents tend to generate toxic sludge, which has to be removed prior to further treatment [11]. Additionally, flocculation or precipitations technologies involve the use of chemicals that have to be removed before consumption. Ion exchange processes are generally non-specific to the ion removed and tend to be expensive. Whereas, adsorption techniques have shown much promise for the remediation of metals from water. In addition, the use of nano-sized adsorbents with high surface area have shown great increases reactivity and binding capacities for metal ions. Adsorption technologies tend to be more cost-effective technologies and less complicated to implement.

Many adsorbents have been investigated for their capabilities to remove heavy metal ions from water, examples include: iron oxides, iron sulfides, aluminum oxides, graphene oxides, zinc oxides, granular ferric oxides (GFO's), copper oxides, sawdust, biochar, pomegranate biosorbent, titanium dioxide, manganese oxides, red mud, activated carbon, and many other types of materials [7-8, 13-20]. Although there are several materials with high binding affinities, iron-based nanomaterials are of great interest due to their magnetic properties. In recent studies, Fe_2O_3 and Fe_3O_4 showed promising results in removing both Pb^{2+} and Cu^{2+} from aqueous solutions [8]. Tamez et al. showed that Fe_2O_3 had a binding capacity of 47.62 mg/g and 19.61 mg/g for Pb^{2+} and Cu^{2+} ions, respectively within 1 hr contact with the

adsorbent. Additionally, Fe_3O_4 had capacities of 166.67 mg/g and 37.04 mg/g for Pb^{2+} and Cu^{2+} ions, respectively within 1 hr of contact with the adsorbent [8]. Furthermore, Sitko et al. showed that graphene oxide had capacities of 1119 mg/g and 294 mg/g for Pb^{2+} and Cu^{2+}, respectively [16]. On the other hand, Mahdavi et al. proved that ZnO had high capacities of 112.7 mg/g and 137.5 mg/g for Pb^{2+} and Cu^{2+} [18]. In the same study, CuO was found to have lower capacities of 14.2 mg/g and 54.1 mg/g for both Pb^{2+} and Cu^{2+} ions [18]. Similarly, graphene oxide showed to have a capacity of 117.5 mg/g with 2.5 hr of contact time [7].

In the present study, pyrrhotite, (Fe_7S_8), was synthesized and studied for the removal of lead^{2+} and copper^{2+} ions from aqueous solutions. The nanomaterial was synthesized using a solvothermal process. mixing mixture of 60 mM thiourea and 30 mM iron(III) chloride hexahydrate was added to a mixture of ethylene glycol and 18 Ω H_2O. The mixture was reacted at 180°C in a Teflon lined stainless steel autoclave. The synthesized material was characterized using X-ray diffraction, which confirmed the correct phase with a crystallite size of 29.86 ± 0.87 nm. Various batch studies were performed to determine the effects of pH, time, temperature, binding capacity, and thermodynamics of the binding process. As well, studies were performed to determine the effects of common hard cations found in natural water systems on the binding process.

2. Methodology

2.1 Synthesis of nanomaterial

The synthesis of the pyrrhotite (Fe_7S_8) nanomaterial was conducted using a solvothermal method similar to the method used by Zhang and Chen [21]. In brief, 60 mmol of thiourea (Acros Organics) and 30 mmol of iron (III) chloride hexahydrate ($FeCl_3{\cdot}6H_2O$; Acros Organics) were dissolved in a mixture of 60 mL of ethylene glycol and 20 mL of Millipore water (18Ω). The reaction mixture was then transferred into Teflon lined autoclaves (the autoclaved were filled to approximately 80% of the capacity). The autoclaves were sealed and placed in the oven at 180°C and reacted for 1hr. Subsequent to reaction, the autoclaves were allowed to cool naturally to room temperature. The products were then filtered and washed using alternating washes of methanol and acetone to remove any contaminants/ byproducts from the reaction.

2.2 X-ray diffraction analysis

The synthesized Fe_7S_8 was characterized using X-ray diffraction. The diffraction patterns were collected using a Rigaku Miniflex Diffractometer. The product was ground into a fine powder using a mortar and pestle. The sample was placed on a Al sample holder. The XRD patterns were collected using the Cu kα (1.54 Å), a nickel filter, the data range was from 20° to 60° (in 2θ), a step width of 0.05°, and a 5s counting time,. From the analysis, the average particle size was determined using a Gaussian fitting for three independent diffraction peaks and Scherrer's equation. A Le Bail fitting of the X-ray diffraction pattern was performed using the FullProf 2001 Suite of programs and crystallographic data from the literature [22-24].

2.3 pH profile

The effect of pH on the binding of Pb^{2+} and Cu^{2+} to the Fe_7S_8 was studied from pH 2 to pH 6 using 0.3 mM and 300 ppb solutions of Pb(II) and Cu(II), respectively. The pH adjustments for the 0.3 mM and 300 ppb solutions of Pb^{2+} and Cu^{2+} were done using either dilute trace metal grade nitric acid or dilute sodium hydroxide. 4.0 mL aliquots of the pH-adjusted solutions were transferred to 5-mL polyethylene test tubes, which contained 10 mg of the dried Fe_7S_8. In addition, control reactions were conducted, which consisted of 4.0 mL the pH adjusted lead and copper solutions in empty test tubes. The control samples and reaction samples were equilibrated by continuously rocking the samples for 1 h at room temperature. Furthermore, the reaction and control samples for the Pb^{2+} or Cu^{2+} were reacted in triplicate for statistical purposes. Subsequent to equilibration, the samples and controls were centrifuged at 3500 RPM for 5 min and the supernatants were extracted and stored for further analysis using ICP-OES.

2.4 Time dependency/Kinetic Studies

Time dependency studies were conducted to determine the minimum time required for binding of the Pb^{2+} and Cu^{2+} to the Fe_7S_8 nanomaterial. For these studies, solutions pH adjusted to 5 consisting of either 0.3 mM Pb^{2+} or 30 ppm Cu^{2+}, were reacted with 10 mg of Fe_7S_8 at different time intervals. 4.0 mL aliquots of the solutions were added to 5-mL polyethylene test tubes containing the Fe_7S_8 and were equilibrated at room temperature on a rocker for 5, 10, 15, 30, 60, 90, 120, and 240 min. Furthermore, control samples consisting of the Pb^{2+} or Cu^{2+} solutions in the absence of the Fe_7S_8 were treated in the same manner as the samples. In addition, all reaction and control samples were conducted in triplicate for statistical purposes. In addition, all reactions were performed at three temperatures (4°C, 22°C, and 45°C) to determine the activation energy of the binding. Subsequent to equilibration the samples were centrifuged at 3500 RPM for 5 min, and the supernatants were extracted and stored for further analysis using ICP-OES.

2.5 Capacity/Thermodynamic Studies

Capacity studies were conducted using Pb^{2+} or Cu^{2+} solution with concentrations of 0.3, 3, 30, 100, 300, and 1000 ppm and the Langmuir isotherm model. The Pb^{2+} and Cu^{2+} solutions were pH adjusted to pH 5, the optimum binding pH (as determined from pH studies). 4.0 mL aliquots of the pH adjusted solutions were transferred to clean 5-mL polyethylene test tubes containing 10 mg of Fe_7S_8 (pyrrhotite) and equilibrated at room temperature for 1h. For the determination of the thermodynamic parameters the isotherm reactions were repeated at temperatures of 4°C and 45°C. The reaction control which contained only Pb^{2+} or Cu^{2+} ions were treated in the same manner as the reaction samples. Each of the concentrations was replicated in triplicate. After equilibration, the samples were centrifuged at 3500 RPM for 5 min, and the supernatants were decanted and stored for further analysis using ICP-OES.

2.6 Interference studies

The binding of Pb^{2+} and Cu^{2+} ions was tested with common cations as possible interferences to the binding process. This study consisted of testing the effects of various concentrations of Na^+, K^+, Mg^{2+}, and Ca^{2+} added to the 0.3 mM Pb^{2+} or 300 ppb Cu^{2+}

solutions. The concentrations for the cations were: 0.3, 3, 30, 100, 300, and 1000 ppm. After pH adjusting to the optimum binding pH, 4.0 mL aliquots of the solutions were transferred into 5-mL polyethylene test tubes, which contained 10 mg of the Fe_7S_8 nanomaterial. The samples were equilibrated for 1 h at room temperature. In addition, control samples containing the ions in solution alone were prepared and treated in the same manner as the reaction samples. All the reaction samples and control samples were prepared in triplicate; for statistical purposes. Subsequent to equilibration, the samples were centrifuged at 3500 RPM for 5 min, and the supernatants were decanted and stored for further analysis using ICP-OES.

2.10 ICP-OES parameters

All ICP-OES analysis was performed using a Perkin Elmer Optima 8300 ICP-OES (Perkin Elmer, Shelton CT) and the Winlab32 software. The parameters used for the ICP-OES analysis are shown in Table 1. Any samples outside of the calibration range of the ICP-OES were diluted to be within the values used for the calibration of the instrument. All results for the Cu^{2+} and Pb^{2+} concentrations were obtained with calibration curves with correlation coefficients (R^2) of 0.99 or better.

3.0 Results and Discussion

3.1 X-ray Diffraction

From the diffraction pattern shown in Figure 1, the material synthesized consists of two phases: Fe_7S_8 (Pyrrhotite) and Fe_3S_4 (greigite). The majority of the material was determined to be Fe_7S_8, which was approximately 90% of the material and the remaining 10% consisted of the greigite. Fe_7S_8 is found in a monoclinic crystal with a space group of C2/C. The following refined lattice parameters: a=12.00185 Å, b=6.88428 Å, c=13.18790 Å, with a=c=90° and b=119.419°, which corresponded to the literature values were determined using the LeBail fitting procedure and the Fullprof software [22,25]. On the other hand the Fe_3S_4 is a cubic crystal with a space group of FD3M. Using the LeBail fitting procedure in the Fullprof software and crystallographic data from the literature the lattice parameters were refined to a=b=c=9.96841 Å with a=b=c=90°, [26]. The χ^2 of the fitting was determined to be 0.611 showing excellent agreement between the fitting and experimental data. The Bragg peaks in the lower position on the plot correspond to the Fe_3S_4 phase; whereas the higher Bragg peaks are the Fe_7S_8 phase. In addition, the average particle size for the Fe7S8 phase was calculated using Scherer's equation to be 23.3 nm based on the diffraction peak located at 35.04° in 2θ, which corresponds to the 023 plane of the crystal. Similarly, the average particle size for the greigite phase was determined to be 18.7 nm based on the diffraction peak at 36.04°in 2θ which corresponds to the 400 plane in the crystal.

3.2 pH profile studies

Figure 2 show the binding of Pb^{2+} and Cu^{2+} to the Fe_7S_8 nanomaterial from pH 2 to pH 6, respectively. As can be seen in Figure. 2 the binding of the Cu^{2+} ions was unaffected by change in pH, the binding was constant at 100%. However, the binding of lead to Fe_7S_8 was affected greatly with change in pH. At pH 2 the observed binding was found to be below 5 percent and the binding was observed to improve with increasing in pH with a maximum

observed binding of 67% at a pH 6. A pH of 5 was selected as the optimal binding pH for both ions for all further studies, due to the possibility of the precipitation of Pb^{2+} and Cu^{2+} ions through the formation of hydroxides. The results of the pH profile studies are in agreement with other studies in the literature for lead binding to other nanomaterials [7,8,15,16,27,28]. For example, Fe_3O_4 nanomaterial have shown similar increases in binding with increasing pH for the binding of Pb^{2+} ions from solution. Other materials with similar binding trends include; CuO, graphene oxide, meranti wood, and zero valent iron particles [14,18,20]. Tamez, et al. showed the adsorption of Pb^{2+} and Cu^{2+} to Fe_3O_4 and Fe_2O_3. In the study, the binding of Pb^{2+} to the Fe_3O_4 was observed to be low at pH 2 and became pH independent at pH 3 and above. However, Cu^{2+} was observed to be pH dependent showing an increase in the binding with an increasing pH. The binding of Cu^{2+} to the Fe_2O_3 nanoparticles show low binding at pH 2 and became pH independent at pH 3 and above; however, the binding of Pb^{2+} was observed to have the opposite trend with the observed binding decreasing above pH 3 [8]. Mahdavi et al. studied the removal of Pb^{2+} and Cu^{2+} using Fe_3O_4, ZnO, and CuO. In this study, the effects of the pH were tested using 100 ppm solutions of the ions. The results showed that for Fe_3O_4 and CuO, the binding of both ions increased with increasing pH, but the binding for both Pb^{2+} and Cu^{2+} to ZnO was observed to be relatively pH independent [18].

3.3 Kinetics and Activation Energy Studies

The results from the kinetics studies for Pb^{2+} and Cu^{2+} binding to the Fe_7S_8 nanomaterial are shown in Table 2. As can be seen in Table 2, the binding of Pb^{2+} was found to be dependent on time and temperature. As can be seen in Table 2 the binding of Cu^{2+} increased with increasing time and increased with temperature. The binding of Cu^{2+} at all three temperatures started with a small rate constant (slope of the line) which increased with increasing temperature from 4°C to 45°C. Direct dependencies on time were observed for the binding of both Pb^{2+} and Cu^{2+} to the Fe_7S_8 nanomaterial. In addition, the data suggests that the binding follows a zeroth order reaction for the binding. The data also suggests the binding is endothermic in nature as the rate increased with increasing temperature and so to did the percentage removal. Similar trends have been observed in the literature for the removal of Pb^{2+} and Cu^{2+} with various metal oxides and nanomaterials [15,16,18,21,29-32].

The data obtained from the kinetics studies at different temperatures allows for the determination of the activation energy for the binding. The use of the Arrhenius equation shown below

$$Ln(k) = -\frac{E_a}{RT} + Ln(a) \quad 1$$

Where the Ln(k) is the natural log of the rate constant for the reaction, E_a is the activation energy, R is the gas constant 8.314 J/mol K, T is the temperature of the reaction in Kelvin, and the Ln(a) is the frequency factor for the reaction. By plotting the Ln(k) determined from the kinetics reactions from different temperatures against 1/T in Kelvin the Arrhenius plot is developed. The Arrhenius plot developed for the binding of both Pb^{2+} and Cu^{2+} to the Fe_7S_8

nanomaterial is shown in Figure 2. Where the slope is equal to $-E_a/R$. Studies have shown the Activation energy required for binding for both Pb^{2+} and Cu^{2+} are general close to each other with activation energies of of approximately 23 and 45 kJ/mol, respectively. In addition, studies have shown that activation energies in the range of 4.2 to 80 kJ/mol are indicative of chemisorption [33]. Whereas, activation energies below 4.2 kJ/mol are indicative of physisorption [33]. The results of the Activation energy studies are presented in Table 2, as can be seen the activation energies for Pb^{2+} and Cu^{2+} very close as to each other they only differ by 15 kJ/mol. The activation energies determined for the binding of Pb^{2+} and Cu^{2+} indicate the reaction may be occurring via chemisorption. As mentioned earlier for chemisorption it has been shown the chemisorption occurs with activation energies in the range of 4.2 kJ/mol to 80 kJ/mol [33].

3.5 Capacity and Thermodynamics study

The results of the capacity studies are shown in Table 3 for the binding of both Pb^{2+} and Cu^{2+} to the Fe_7S_8 nanomaterial with 1 h contact time. The capacity studies were performed at three different temperatures 4° 21°C, and 45°C. The binding for both Pb^{2}+ and Cu^{2+} ions was found to follow the Langmuir isotherm model. As can be seen in in Table 3 an increase in binding capacity is observed with an increase in reaction temperature. At 4°C, the nanomaterial showed a higher adsorption capacity for Pb^{2+} (6.23 mg/g) in which its capacity was five times that of copper (1.31 mg/g) whereas at 45°C, the adsorption capacity for copper (116.3 mg/g) was approximately five times that of lead (21.4 mg/g).

Recent studies have shown variable results for the adsorption of Pb^{2+} and Cu^{2+} to other nanomaterials [7,15-16,34]. For instance, graphene oxide has been shown to have high binding capacities of 294, 530, 345, 1119 mg/g for Cu^{2+}, Cd^{2+}, Zn^{2+}, and Pb^{2+} respectively [16]. However, binding capacity results for Fe-water treatment residues have been observed to be in the same range as the present study for Pb^{2+} and Cu^{2+} with 22 mg/g and 6mg/g, respectively [34]. In addition, Red mud has also shown similar adsorption capacities for Cu_{2+} with a maximum capacity of 5.3493 mg/g [35]. Whereas, activated carbon synthesized using Pine cones showed an adsorption capacity of 27.53 mg/g for the adsorption of Pb^{2+} [36]. Table 4 presents adsorption capacities for the removal of Pb^{2+} and Cu^{2+} using different materials. The capacity of Fe_3O_4 has been observed to change with respect to the Fe_3O_4 particle size; where the smaller the particle size, the higher the binding capacity for both Pb^{2+} and Cu^{2+} are observed. For example, Fe_3O_4 with a particle size of 50 nm showed a capacity of 101.4 and 14.7 mg/g, respectively; furthermore Fe_3O_4 with a particle size of 12.9 ± 1.4 nm had binding capacities of 166.67 and 37.04 mg/g for Pb^{2+} and Cu^{2+}, respectively [8,18].

The data obtained from the thermodynamic study was used to determine Gibbs free energy, enthalpy, and entropy of the system, which are shown in Table 5. The change in Gibbs free energy was calculated for both Pb^{2+} and Cu^{2+} at three different temperatures. The relationships between ΔG, ΔH, ΔS, and LnK_d are shown in Eqs. (2) and (3).

$$\Delta G = -RTLn(k_d) \quad (2)$$

$$Ln(k_d) = \frac{\Delta S}{R} - \frac{\Delta H}{RT} \quad (3)$$

In which the ΔG is the Gibbs free energy; R is the gas constant (8.314 J K^{-1} mol^{-1}); T is the absolute temperature in Kelvin; K_d is the distribution coefficients; ΔS is the change in entropy; ΔH is the change in enthalpy. The ΔH and ΔS were determined by plotting the LnK_d against 1/T (in K) the slope of the line and intercept of the plot are related to the ΔH and ΔS of reaction, respectively. The thermodynamic plots are shown in Figure 4. In addition, the calculated thermodynamic parameters ΔG, ΔH and ΔS are shown in Table 5. According to the results, the binding of the system for Pb^{2+} gets more spontaneous as the temperature increases as well this same trend was observed for the Cu^{2+} binding. The increased binding capacity and the increased spontaneity of the reaction corroborate the data observed in the kinetics study, that an endothermic reaction is taking place during the binding process for both the Pb^{2+} and Cu^{2+} ions. In a previous study conducted by Ahmad et al., the binding of the system for both ions was spontaneous due to a negative ΔG for both Pb^{2+} and Cu^{2+}. For instance, the ΔG for the binding of lead and copper onto sawdust from meranti wood decreased from −20.99 to −25.16 kJ/mol and −21.09 kJ/mol to −26.40 kJ/mol, respectively with increasing temperature [14]. In another study conducted by Ben-Ali, et. al, the adsorption process of Cu^{2+} onto pomegranate peel was determined to be spontaneous at high temperatures. In the study, the ΔG for the sorption at 303 K and 313 K was −5.358 kJ/mol and −7.409 kJ/mol, respectively [37]. Additionally, a study conducted by A. Sonmezay et al, studied the sorption process for Pb^{2+} using manganese oxide minerals, which consisted of a mixture of MnO_2, CaO, SiO_2, TiO_2, Al_2O_3, Fe_2O_3, K_2O, and MgO. The ΔG for the binding at 298 K, 308 K, and 318 K was −27.69 kJ/mol, −28.81 kJ/mol, and −29.84 kJ/mol, respectively [38]. Whereas, Zou, et al., studied the adsorption of Cu^{2+} and Pb^{2+} using manganese oxide coated zeolite. This study observed for both Pb^{2+} and Cu^{2+} ions at 288 K, 303 K, and 313 K were −50.5 kJ/mol, −53.6 kJ/mol, and −56.7 kJ/mol and −50.5 kJ/mol, −53.5 kJ/mol, and −56.5 kJ/mol for Cu^{2+}, respectively [32]. In the present study, ΔG for the sorption process of Pb was 5.07 kJ/mol (277 K), 1.43 kJ/mol (295 K), and −2.45kJ/mol (318 K) whereas for Cu, the ΔG was 9.7 kJ/mol (277 K), 4.4 kJ/mol (295 K), and −11.22 kJ/mol (318 K). Furthermore, the ΔG values found in the present study were relatively close to zero indicating that the process was near equilibrium. The results from the present study are in agreement with the literature indicating an endothermic reaction occurs with the binding of a metal ion to a mineral/nanomaterial surface.

The ΔH and ΔS were both determined by plotting LnK_d vs 1/T (in K), which is shown in Figure 4. From the plot, ΔH was determined from the slope of the line whereas ΔS was determined from the intercept of the plot. The values for both the ΔH and ΔS are presented in Table 5. The ΔH for the sorption of Pb^{2+} indicates an endothermic reaction occurs for the binding of to the Fe_7S_8, the high positive value of 55.8 kJ/mol. Similarly, the ΔH for the binding of Cu^{2+} indicates an endothermic reaction a very high positive value of 153.5. These values indicate that the sorption for both the Pb^{2+} and Cu^{2+} occurs through similar processes and endothermic reaction. According to the ΔH, the binding of Pb^{2+} and Cu^{2+} both occur through chemisorption. The ΔH of chemisorption for binding has been shown in the

literature to be greater than 40 kJ/mol [39]. Furthermore, the ΔS of the binding for both Pb^{2+} and Cu^{2+} were positive values of 183.6 and 515.5 J/mol indicating that there an increase decrease of entropy in the system after the reaction. An increase in entropy for a reaction generally indicates a favorable process.

3.9 Interferences studies

Figure 5a and Figure 5b show the results for the individual and combined interference study for the binding of Pb^{2+} and Cu^{2+} to the Fe_7S_8 nanomaterial, respectively. The binding interferences used for both Pb2+ and Cu2+ were common cations found in natural water systems. The interferences were Na^+, K^+, Ca^{2+}, and Mg^{2+} were investigated keeping the Pb^{2+} and Cu^{2+} concentration constant and increasing the interference concentrations. The combined interference studies consisted of all four cations present in solution at the same concentration. For example the 1000 ppm interference solution consisted of 1000 ppm of Na +, 1000 ppm K^+, 1000 ppm Ca^{2+} and 1000 ppm Mg^{2+}, giving a total interference concentration of 4000 ppm, with a either a Pb^{2+} concentration of 0.3 mM or a Cu^{2+} concentration of 300 ppb. At a 1000 ppm of each interfering ion a molar ratio of 1:452 is observed for Pb^{2+}: interference and 1:318 for Cu^{2+}: interference From Figure 5a, it can be seen that in the presence of Na^+, there was little to no change in the binding from 0.3 ppm to 100 ppm. However, at higher concentrations a synergistic effect occurred where the binding of Pb^{2+} increased by 10%. In the presence of the other cations: K^+, Mg^{2+}, and Ca^{2+}, the binding of Pb^{2+} was observed to have little to no change as the concentration of the interferences increased. The binding of lead in the combined interference study (presence of all four cations Na^+, K^+, Mg^{2+}, Ca^{2+}) showed little to no change as the concentrations increased. Similarly, Tamez et al., determined that no interference occurred with the binding of Pb^{2+} to Fe_3O_4 nanomaterial, similarly the binding of Pb^{2+} to Fe_2O_3 was unaffected in the presence of K^+ and Mg^{2+}. However, the presence of Na^+ or Ca^{2+} was shown to increase the binding of lead to Fe_2O_3 [8].

As can be seen in Figure 5b, the presence of Na^+, Mg^{2+}, and Ca^{2+} had an antagonistic effect on the binding of Cu^{2+} to the Fe_7S_8 nanomaterial as the concentration of the hard cations increased. The binding for Cu^{2+} in the presence of Na^+ was observed to decrease from 97% at a concentration of 0.3 ppm to approximately 87% at a Na^+ concentration of 1000 ppm. The binding of Cu^{2+} in in the presence of Mg^{2+} and Ca^{2+} decreased by approximately 40% and 30%, respectively, with interference concentrations from 3 to 1000 ppm. On the other hand, K^+ had little to no effect on the binding of Cu^{2+} to the Fe_7S_8 nanomaterial. However, in the combined interference study the binding of Cu^{2+} in decreased by approximately 40% between the inferences concentrations of 3 and 1000 ppm of the cations. Tamez et al., found that the binding of Cu^{2+} to Fe_3O_4 was unaffected in the presence of any cation; whereas in the binding to Fe_2O_3, Mg^{2+} had an antagonist effect, the binding of the Cu^{2+} decreased as the concentration of Mg^{2+} increased. However, in the presence of Ca^{2+} a synergistic effect was observed showing the binding of Cu^{2+} increased as the concentration of Ca^{2+} increased [8].

4. Conclusions

The binding of Pb^{2+} to the Fe_7S_8 was determined to be pH dependent whereas the binding of Cu^{2+} was determined to be pH independent. The Pb^{2+} had a low binding at pH 2 but steadily increased with an increase in pH. The binding of both Pb^{2+} and Cu^{2+} were found to be time dependent and were determined to follow zeroth order kinetics. The reaction between Pb^{2+} and Fe_7S_8 was determined to be nonspontaneous at low temperatures and endothermic. Similarly, the binding of Cu^{2+} to Fe_7S_8 was determined to be non-spontaneous at low temperatures and endothermic. The ΔG for both Pb^{2+} and Cu^{2+} were relative close to zero indicating that the reaction was close to equilibrium. At the low temperature the Cu^{2+} had a binding capacity of approximately twice that of the Pb^{2+} ions to the Fe_7S_8 nanomaterial. At room temperature Cu^{2+} exhibited approximately 2.5 times the binding capacity observed for Pb^{2+}. The Cu^{2+} showed a binding capacity approximately 20 times that of Pb^{2+} at 45°C with 1.92 mmol/g and 0.103 mmol/g, respectively.

Acknowledgments

Authors would like to thank the NIH UTRGV RISE program (Grant Number 1R25GM100866-03). The Authors acknowledge financial support from the Welch Foundation for supporting the Department of Chemistry (Grant number GB-0017).

References

1. Hoekstra AY, Mekonnen MM. Global Water Scarcity: The monthly blue water footprint compared to blue water availability for the world’s major river basins. 2011Value of Water Research Report Series No. 53
2. Needleman H. Lead Poisoning. Annual Review of Medicine. 2004; 55:209–222.
3. Tong S, von Schirnding YE, Prapamontol T. Environmental lead exposure: a public health problem of global dimensions. Bulletin of the World Health Organization. 2000; 789:1068–1077. [PubMed: 11019456]
4. World Health Organization. Lead in drinking-water: background document for development of WHO guidelines for drinking-water quality. WHO. 1996
5. Eren E, Afsin B, Onal Y. Removal of lead ions by acid activated and manganese oxide-coated bentonite. Journal of Hazardous Materials. 2009; 161:677–685. [PubMed: 18501507]
6. Gaetke LM, Chow CK. Copper toxicity, oxidative stress, and antioxidant nutrients. Toxicology. 2003; 189:147–163. [PubMed: 12821289]
7. Wu W, Yang Y, Zhou H, Ye T, Huang Z, Liu R, Kuang Y. Highly efficient removal of Cu(II) from aqueous solution by using graphene oxide. Water Air Soil Pollut. 2013; 224:1372.
8. Tamez C, Hernandez R, Parsons JG. Removal of Cu (II) and Pb (II) from Aqueous solution using engineered iron oxide nanoparticles. Microchemical Journal. 2016; 125:97–104. [PubMed: 26811549]
9. Georgopoulos PG, Wang SW, Georgopoulos IG, Yonone-lioy MJ, Lioy PJ. Assessment of human exposure to copper: a case study using the NHEXAS database. Journal of Exposure Science and environmentaly epidemiology. 2006; 16:397–409.
10. Mosayebi E, Azizian S. Study of copper ion adsorption from aqueous solution with different nanostructured and microstructured zinc oxides and zinc hydroxide loaded on activated carbon cloth. Journal of Molecular Liquids. 2016; 214:384–389.
11. Fu F, Wang Q. Removal of heavy metal ions from wastewaters: A review. Journal of Environmental Management. 2011; 92:407–418. [PubMed: 21138785]
12. Anthemidis AN, Ioannou KG. Recent developments in homogeneous and dispersive liquid-liquid extraction for inorganic elements determination. A review Talanta. 2009; 80:413–421. [PubMed: 19836497]

13. Liu Y, Chen L, Li Y, Wang P, Dong Y. Synthesis of magnetic polyaniline/graphene oxide composites and their applications in the efficient removal of Cu(II) from aqueous solutions. Journal of Environmental Chemical Engineering. 2016; 4:825–834.
14. Ahmad A, Rafatullah M, Sulaiman O, Ibrahim MH, Chi YY, Siddique BM. Removal of Cu(II) and Pb(II) ions from aqueous Solutions by adsorption on sawdust of meranti wood. Desalination. 2009; 247:636–636.
15. Farghali AA, Bahgat M, Enaiet Allah A, Khedr MH. Adsorption of Pb(II) ions from aqueous solutions using copper oxide nanostructures. BENI-SUEF University Journal of Basic and Applied Sciences. 2013; 2:61–71.
16. Sitko R, Turek E, Zawisza B, Malicka E, Talik E, Heimann J, Gagor A, Feist B, Wrzalik R. Adsorption of divalent metal ions from aqueous solutions using graphene oxide. Dalton Trans. 2013; 42:5682–5689. [PubMed: 23443993]
17. Wang X, Chen Z, Yang S. Applications of graphene oxides for the removal of Pb(II) ions from aqueous solutions: Experimental and DFT calculation. Journal of Molecular Liquids. 2015; 211:957–964.
18. Mahdavi S, Jalali M, Afkhuami A. Removal of heavy metals from aqueous solutions using Fe3O4, ZnO, and CuO nanoparticles. Journal of Nanoparticle Research. 2012; 14:846.
19. Wang H, Gao B, Wang S, Fang J, Xue Y, Yang K. Removal of Pb(II), Cu(II), and Cd(II) from aqueous solutions by biochar derived from $KMnO_4$ treated wood. Biosource Technology. 2015; 197:356–362.
20. Azzam AM, El-Wakeel ST, Mostafa BB, El-Shahat MF. Removal of Pb, Cu, and Ni from aqueous solution using nano scale zero valent iron particles. Journal of Environmental Chemical Engineering. 2016; 4:2196–2206.
21. Zhang ZJ, Chen XY. Magnetic greigite (Fe3S4) nanomaterials: shape- controlled solvothermal synthesis and their calcination conversion into hematite (a-Fe2O3) nanomaterials. J Alloys Compd. 2009; 488:339–345.
22. Lebail A, Duroy H, Fourquet JL. AB-initio structure of LiSbWO8 by X-ray powder diffraction. Mater Res Bull. 1988; 23:447–452.
23. Carvajal JR. Physica B. 1993; 192:55.
24. Cantu J, Gonzalez LE, Goodship J, Contreras M, Joseph M, Garza C, Eubanks TM, Parsons JG. Removal of arsenic from water using synthesic Fe_7S_8 nanoparticles. Chemical Engineering Journal. 2016; 290:428–437. [PubMed: 27065750]
25. Tokonami M, Nishiguchi K, Morimoto N. Crystal structure of a monoclinic pyrrhotite (Fe7S8). Am Mineral. 1972; 57:1066–1080.
26. Skinner BJ, Erd RC, Grimaldi FS. Greigite, the thio-spinel of iron: a new mineral. Am Mineral. 1964; 49:543–555.
27. Fan Q, Li Z, Jia HZ, Xu J, Wu W. Adsorption of Pb(II) on palygorskite from aqueous solution: Effects of pH, ionic strength and temperature. Applied Clay Science. 2009; 45:111–116.
28. Gadde RR, Laitinen HA. Studies of heavy metal adsorption by hydrous iron and manganese oxides. Analytical Chemistry. 1974; 46(13):2022–2026.
29. Fouladgar M, Beheshti M, Sabzyan H. Single and binary adsorption of nickel and copper from aqueous solutions by γ-alumina nanoparticles: Equilibrium and kinetic modeling. Journal of Molecular Liquids. 2015; 211:1060–1073.
30. Chen YH, Li FA. Kinetic study on removal of copper(II) using goethite and hematite nano-photocatalysts. Journal of Colloid and Interface Science. 2010; 347:277–281. [PubMed: 20430397]
31. Gupta VK, Rastogi A. Biosorption of lead from aqueous solutions by green algae Spirogyra species: Kinetics and equilibrium studies. Journal of Hazardous Materials. 2008; 152:407–414. [PubMed: 17716814]
32. Zou W, Han R, Chen Z, Jinghua Z, Shi J. Kinetic study of Cu(II) and Pb(II) from aqueous solutions using manganese oxide coated zeolite in batch mode. Colloids and Surfaces A: Physicochem. Eng Aspects. 2006; 279:238–246.

33. Mahmood T, Saddique MT, Naeem A, Mustafa S, Zeb N, Shah KH, Waseem M. Kinetic and thermodynamic study of Cd(II), Co(II) and Zn(II) adsorption from aqueous solution by NiO. Chem Eng J. 2011; 171:935–940.

34. Castaldi P, Silvetti M, Garau G, Demurtas D, Deiana S. Copper(II) and lead(II) removal from aqueous solution by water treatment residues. Journal of hazardous materials. 2015; 283:140–147. [PubMed: 25262486]

35. Nadaroglu H, Kalkan E, Demir N. Removal of copper from aqueous solution using red mud. Desalination. 2010; 251:90–95.

36. Momcilovic M, Purenovic M, Bojic A, Zarubica A, Randelovic M. Removal of lead(II) ions from aqueous solutions by adsorption onto pine cone activated carbon. Desalination. 2011; 276:53–59.

37. Ben-Ali S, Jaouali I, Souissi-Najar S, Ouederni A. Characterization and adsorption of raw pomegranate peel biosorbent for copper removal. Journal of Cleaner Production. 2017; 142:3809–3821.

38. Sonmezay A, Oncel MS, Bektas N. Adsorption of Lead and Cadmium Ions from Aqueous solutions using manganoxide minerals. Transactions of Nonferrous Metals Society of China. 2012; 22:3131–3139.

39. Al-Anber MA. Thermodynamics approach in the Adsorption of heavy metals. Intech. 2011

40. Asuquo E, Martin A, Nzerem P, Siperstein F, Fan X. Adsorption of Cd(II) and Pb(II) ions from aqueous solutions using mesoporous activated carbon adsorbent: Equilibrium, kinetics, and characterisation studies. Journal of Environmental Chemical Engineering. 2017; 5:679–698.

41. Hua M, Zhang S, Pan B, Zhang W, Lv L, Zhang Q. Heavy metal removal from water/wastewater by nanosized metal oxides: A review. Journal of Hazardous Materials. 2012; 211-212:317–331. [PubMed: 22018872]

42. Wang SG, Gong WX, Liu XW, Yao YW, Gao BY. Removal of lead(II) from aqueous solution by adsorption onto manganese oxide-coated carbon nanotubes. Separation and Purification Technology. 2007; 58:17–23.

Highlights

- A Fe_7S_8 nanomaterial was synthesized solvothermally using $FeCl_36H_2O$ in a mixture of ethylene glycol and water
- The binding of both Pb^{2+} and Cu^{2+} ions from aqueous solution to the Fe7S8 nonmaterial were tested
- The Binding parameters investigated included pH, kinetics (time dependency), and thermodynamics
- Hard cations showed little to no effect on both Pb^{2+} and Cu^{2+} ions to the Fe_7S_8 nanomaterial

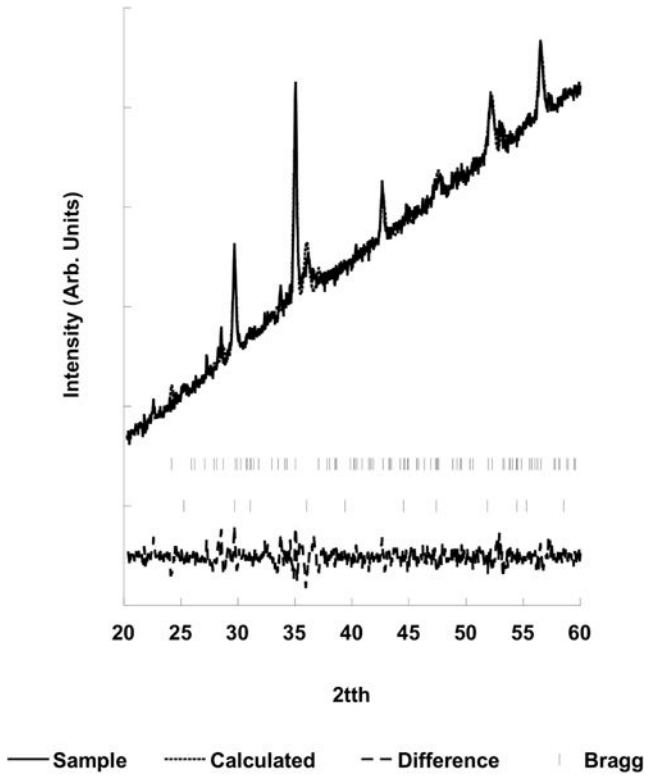

Figure 1.
Powder X-ray diffraction pattern for the iron sulfide nanomaterial as synthesized.

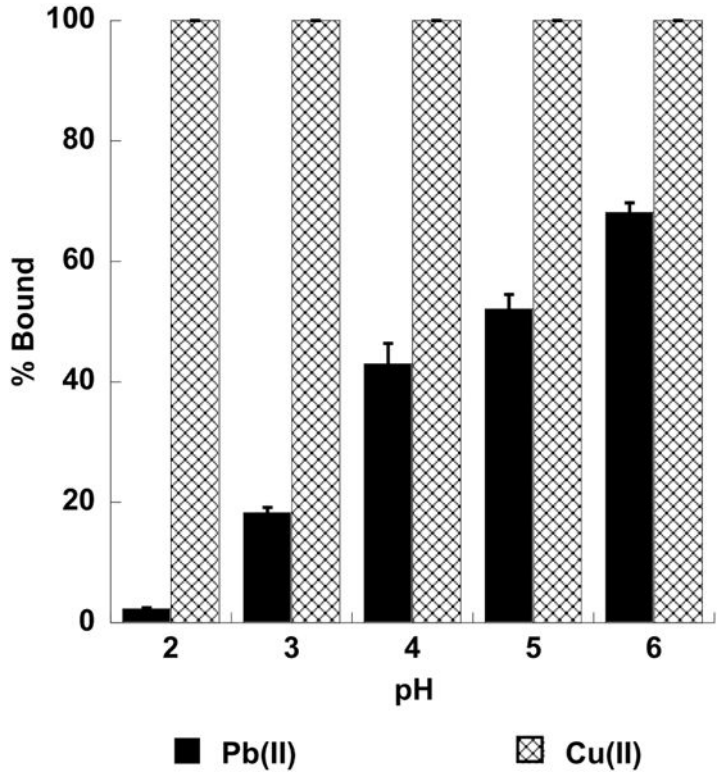

Figure 2.
Effect of pH from 2.0 to 6.0 on the binding of Pb^{2+} andCu^{2+} to the Fe_7S_8 nanomaterial.

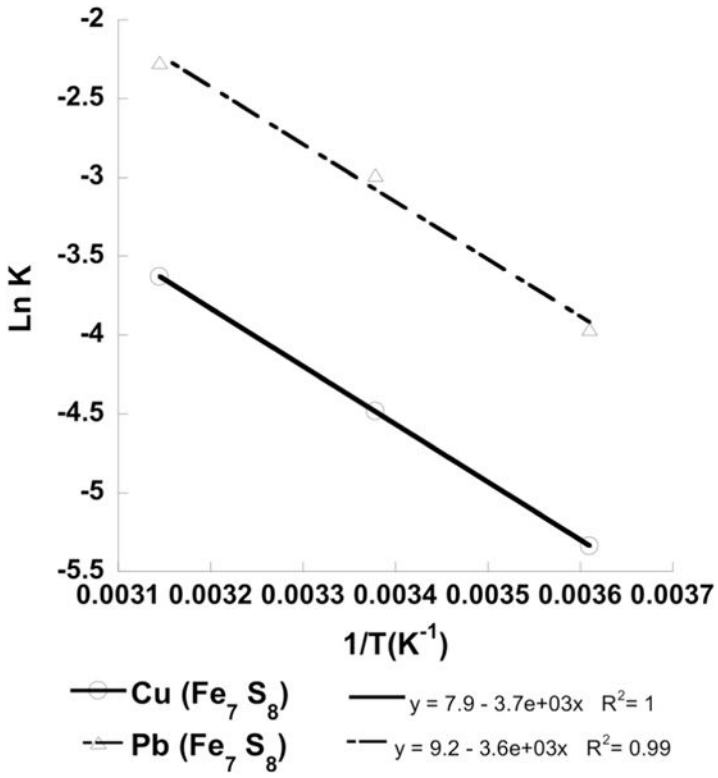

Figure 3.

Arrhenius plot the binding of Pb^{2+} and Cu^{2+} to the Fe_7S_8 at temperatures of 4, 22 and 45°C at the optimal binding pH

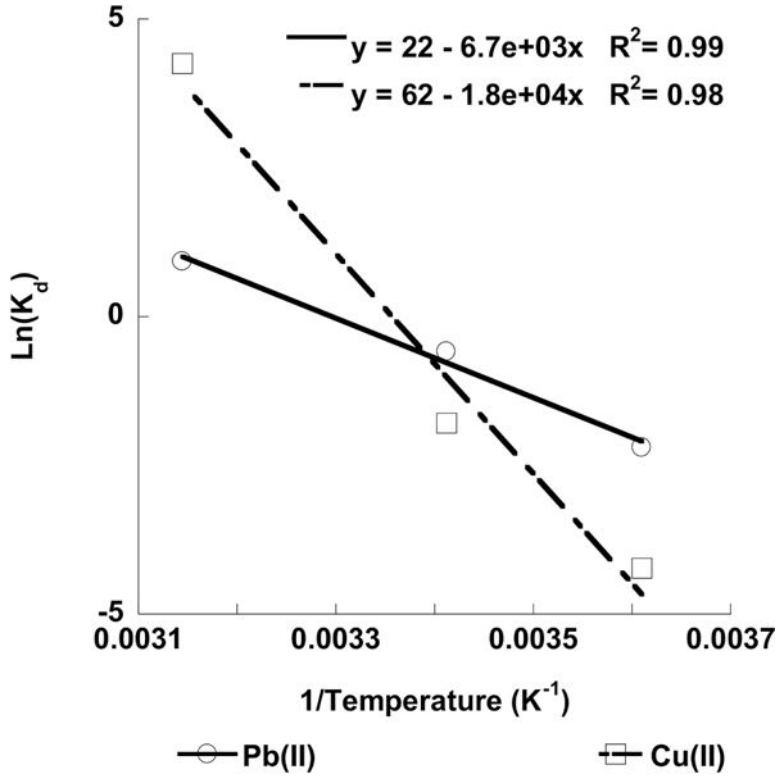

Figure 4.

Thermodynamics plot for the adsorption of of Pb^{2+} and Cu^{2+} to the Fe_7S_8 at temperatures of 4, 22 and 45°C at the optimal binding pH.

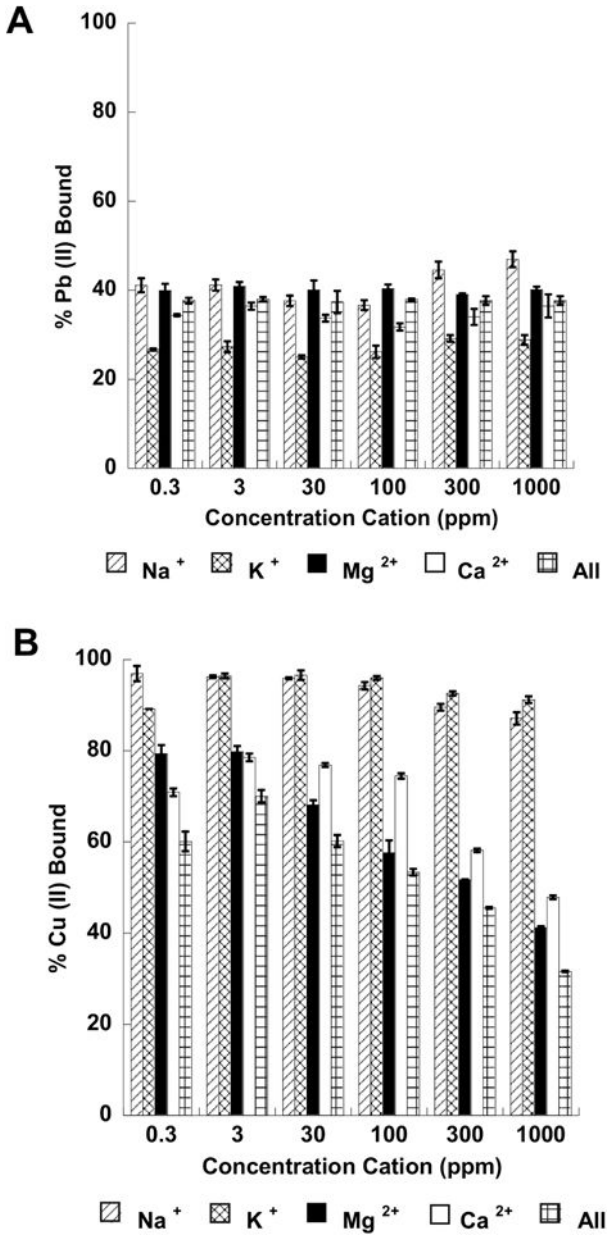

Figure 5.

A. Binding of Pb^{2+} in the presence of individual interfering cationic species and combined cationic species at the optimal binding pH. **B.** Binding of Cu^{2+} in the presence of individual interfering cationic s

Table 1

ICP-OES parameters used for the analysis of Pb(II) and Cu(II) solutions after reaction with the Fe_7S_8 nanomaterial.

Parameter	Settings Pb Cu(II)
λ_{Pb}	217 nm
λ_{Cu}	327.393 nm
RF power	1500 W
Nebulizer	Gemcone (low flow)
Plasma Flow	15 L/min
Auxiliary Flow	0.2 L/min
Nebulizer Flow	0.55 L/min
Sample Flow	1.50 mL/min
Injector	2.0 mm Alumina
Spray Chamber	Cyclonic
Integration Time	20 seconds
Replicates	3

Table 2

Results of kinetics studies and activation energy studies performed at temperatures of 4°C. 22°C, and 45°C.

Ion	Temperature (°C)	Equation	R^2	E_a (kJ/mol)
Pb^{2+}	4	0.0832x+13.49	0.986	
	22	0.1533x+14.04	0.980	23.6
	45	0.3033x+31.519	0.989	
Cu^{2+}	4	0.063x+5.39	0.995	
	22	0.1276x+9.49	0.990	45.1
	45	0.7604x+51.59	0.983	

Table 3

Binding capacity of the Fe_7S_8 nanomaterial for Pb^{2+} and Cu^{2+} using the Langmuir isotherm.

Ion Form	Capacity (mg/g)	Capacity (mmol/g)
Pb^{2+}	6.23 (277)	0.030
	8.09 (298)	0.039
	21.4 (318)	0.103
Cu^{2+}	1.31 (277)	0.073
	5.29 (298)	0.102
	116.3 (318)	1.92

Table 4

Comparison of adsorption capacities for Pb^{2+} and Cu^{2+} binding to various different adsorbents.

Material	Adsorption Capacity (mg/g)	Adsorption capacity (mmol/g)	Ion species	Reference
Graphene Oxide	117.5	1.84	Cu(II)	[7]
Fe(OOH) (goethite)	149.25	2.35	Cu(II)	[30]
Fe_3O_4	166.67	0.81	Pb(II)	[8]
	37.04	0.58	Cu(II)	
Fe_2O_3	47.62	0.23	Pb(II)	[8]
	19.61	0.31	Cu(II)	
Fe_3O_4	101.4	0.49	Pb(II)	[18]
	14.7	0.23	Cu(II)	
ZnO	112.7	0.54	Pb(II)	[18]
	137.5	2.16	Cu(II)	
CuO	39.4	0.19	Pb(II)	[18]
	54.1	0.85	Cu(II)	
$KMnO_4$ modified	153.1	0.74	Pb(II)	[19]
Biochar	34.2	0.54	Cu(II)	
TiO_2	81.3	0.39	Pb(II)	[41]
CeO_2	9.2	0.044	Pb(II)	[41]
	15.4	0.24	Cu(II)	
MnO_2/CNTs	78.74	0.38	Pb(II)	[42]
Red mud	5.35	0.084	Cu(II)	[35]

Table 5

Calculated Thermodynamic Parameters for the adsorption of Pb^{2+} and Cu^{2+} to the nanomaterial.

Ion form	ΔG (kJ/mol)	ΔH (kJ/mol)	ΔS (J/mol)
Pb^{2+}	5.07 (277	55.81	183.6
	1.44 (295 K)		
	−2.45 (318 K)		
Cu^{2+}	9.78 (277 K)	153.51	515.5
	4.60 (295 K)		
	−11.23 (318 K)		